

See discussions, stats, and author profiles for this publication at: <https://www.researchgate.net/publication/262072883>

3D Imaging of Enzymes Working in Situ

ARTICLE *in* ANALYTICAL CHEMISTRY · MAY 2014

Impact Factor: 5.64 · DOI: 10.1021/ac403699h · Source: PubMed

READS

67

6 AUTHORS, INCLUDING:



Frédéric Jamme

SOLEIL synchrotron

84 PUBLICATIONS 539 CITATIONS

[SEE PROFILE](#)



Georges Tawil

Chopin Technologies

4 PUBLICATIONS 52 CITATIONS

[SEE PROFILE](#)



Alain Buléon

French National Institute for Agricultural Res...

187 PUBLICATIONS 7,570 CITATIONS

[SEE PROFILE](#)

¹ 3D Imaging of Enzymes Working in Situ

² F. Jamme,^{*,†,‡} D. Bourquin,[†] G. Tawil,[‡] A. Viksø-Nielsen,[§] A. Buléon,[‡] and M. Réfrégiers[†]

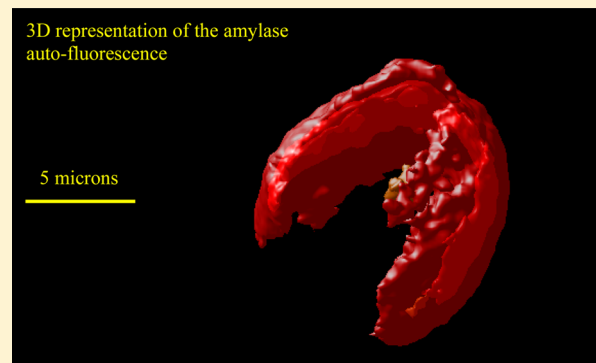
³ [†]Synchrotron SOLEIL, 91190 Saint-Aubin, Gif sur Yvette Cedex, France

⁴ [‡]UR1268 Biopolymères Interactions Assemblages, INRA, F-44300 Nantes, France

⁵ [§]Novozymes A/S, Krogshoejvej 36, 2880 Bagsvaerd, Denmark

⁶ Web-Enhanced Feature

ABSTRACT: Today, development of slowly digestible food with positive health impact and production of biofuels is a matter of intense research. The latter is achieved via enzymatic hydrolysis of starch or biomass such as lignocellulose. Free label imaging, using UV auto-fluorescence, provides a great tool to follow one single enzyme when acting on a non-UV-fluorescent substrate. In this article, we report synchrotron DUV fluorescence in 3-dimensional imaging to visualize in situ the diffusion of enzymes on solid substrate. The degradation pathway of single starch granules by two amylases optimized for biofuel production and industrial starch hydrolysis was followed by tryptophan auto-fluorescence (excitation at 280 nm, emission filter at 350 nm). The new setup has been specially designed and developed for a 3D representation of the enzyme–substrate interaction during hydrolysis. Thus, this tool is particularly effective for improving knowledge and understanding of enzymatic hydrolysis of solid substrates such as starch and lignocellulosic biomass. It could open up the way to new routes in the field of green chemistry and sustainable development, that is, in biotechnology, biorefining, or biofuels.



²³ **W**ith the growing interest for green chemistry, the development of slowly digestible food with positive health impact, that is, stimulating probiotic gut bacteria and the production of biofuels, a fast-expanding research is being performed about enzymatic hydrolysis of biopolymers such as starch and lignocellulose. Contrary to homogeneous phase hydrolysis, where both substrate and enzyme are in solution, the hydrolysis of such solid substrates strongly depends on their complex semicrystalline and hierarchical structure,⁴ which limits the diffusion of enzyme and restricts its accessibility to breakable linkages.

³⁴ Many plants store energy in 1 to 100 μm starch granules. Those granules properties depend on their crystalline ultra-structure.⁵ The starch granule is composed of alternating crystalline and amorphous lamellae repeating in every 9–10 nm.^{5,6} Enzymatic hydrolysis of native starch is involved in many biological and industrial processes as for example starch metabolism in plants, digestion by mammals, malting, fermentation, glucose syrup or bioethanol production. Starch and its two main constituents, amylose and amylopectin, are degraded by α -amylases which are the main enzymes involved in the hydrolysis of $\alpha(1 \rightarrow 4)$ glycosidic bonds.^{7–9} The morphology and the surface of the granule, the amylose content, the crystalline structure or the presence of amylose lipid complexes were earlier shown to be the limiting factors for complete hydrolysis of the starch granule.^{1–4,10–15}

⁴⁹ Recently, two new α -amylases, referred to as AFA and RA, were cloned from *Anoxybacillus flavothermus* and *Rhizomucor* sp., respectively.¹⁶ They were studied for their use in bioethanol

production and low temperature glucose syrup production and were proved to be very efficient in hydrolyzing raw starch granules even in concentrated suspensions ($\leq 31\%$ dry matter).^{17,18} RA is a fungal α -amylase, which contains a starch binding domain (SBD) belonging to CBM20 from the *Aspergillus niger* glucoamylase attached through a glycosylated linker, that has been constructed for starch conversion under SSF conditions during bioethanol production,¹⁶ that is, pH 4.5 and approximately 32 °C. AFA is a bacterial wild type α -amylase which has a SBD belonging to the CBM20 family.¹⁹ In both cases the catalytic mechanism is similar and the catalytic site well conserved as for all known α -amylases. It is well-known that the presence and the size of the SBD-like C domain of amylases is essential for adsorption onto solid starch, which is an important factor for its starch hydrolysis properties. Therefore, the binding capacity and behavior of AFA (a CBM20 attached directly to the catalytic core, that is, no flexible aa linker) and RA (a CBM20 connected to the catalytic core through a flexible aa linker) is different which impacts the hydrolysis mode. The action mode of these two α -amylases has been already thoroughly studied.^{17,18} Their kinetic behavior at different starch concentration, evolution of the morphology, the crystalline structure and the molar mass distribution with the hydrolysis rate has been investigated. Amount of enzyme

Received: November 14, 2013

Accepted: May 5, 2014

76 adsorbed, potential inhibition by oligosaccharides released and
77 formation of unproductive enzyme/substrate complexes or
78 aggregation of enzyme were also assessed. While these results,
79 obtained on a large population of starch granules, are very
80 robust, it is by far much more difficult to extract some
81 representative and quantitative data when considering the
82 behavior of single starch granules. Amylases location at different
83 hydrolysis times within single starch granules was previously
84 determined²⁰ using a setup built at the Synchrotron SOLEIL
85 (Gif sur Yvette, France), which allows to record 2D maps of the
86 tryptophan fluorescence at high spatial resolution (200 nm).
87 However, 2D maps are not sufficient to follow enzymatic
88 degradation because the fluorescence signal is averaged all over
89 the thickness of the whole granule and no information is
90 available in this Z-axis.

91 The present work describes challenging new improvements
92 of the technique including especially high DUV sensibility
93 multi-Z axis acquisition, and subsequent 3D image reconstruc-
94 tion. Thus, application to hydrolysis of maize starch granules by
95 RA and AFA allowing to image, in 3D, the location of these
96 enzymes within the internal parts of starch granules all along
97 their hydrolysis.

98 As always for enzymatic hydrolysis of natural products, there
99 are many factors stemming from the natural variability of starch
100 granules in terms of shape, size or surface and also from damage
101 due to extraction and drying procedures. This may induce some
102 discrepancies between the single granule behavior when
103 compared to a large population of granules. In the same way,
104 smoothness and porosity of the surface, hydration and swelling
105 of the granule, crystallinity and crystalline type, the presence of
106 free chain ends could also differ in a large population of
107 granules. When looking at full field images recorded in visible
108 and fluorescence mode, it is obvious that all starch granules are
109 not degraded synchronously. Therefore, no quantitative and
110 representative values were expected from that synchrotron
111 experiment. But the 3D high resolution UV imaging experiment
112 described here is extremely impactful. It shows clearly the way
113 amylases adsorb onto and diffuse within single starch granules
114 and how it can differ for two very efficient industrial amylases
115 on the same starch source. For the first time the location of
116 amylases can be determined without any probe in 3D, and at a
117 resolution close to that of growth rings, within single raw starch
118 granules all along their hydrolysis.

119 ■ EXPERIMENTAL SECTION

120 **3D Setup.** A full description of the beamline and imaging
121 microscope setup can be found elsewhere.²¹ The monochrom-
122 atized synchrotron beam is coupled to a modified full field
123 microscope (Axio Observer Z1, Carl Zeiss GmbH, Germany)
124 equipped with a cooled Electron Multiplier CCD camera
125 (Hamamatsu C9100–02, Japan). The focusing objective (Zeiss
126 Ultrafluar 40×, Carl Zeiss GmbH, Germany) is axially
127 motorized by the Axio-Observer Z1 microscope. Resolution
128 limit and reproducibility of the axis have been tested and
129 validated with a homemade interferometer. The synchrotron
130 beam exciting the sample may be considered as collimated
131 when entering the microscope. The excitation wavelength was
132 280 nm and emission bandpass filter chosen at 350 nm
133 (XF3000, Omega Optical). The acquisition time was 10 s per
134 emission fluorescence image. Full field 1000 × 1000 pixels
135 images were automatically recorded every 500 nm Z steps over
136 22 μm Z range under μManager control.²² The stack of 251
137 frames are recorded and then the starch granule is restored by

138 PSF deconvolution. To optimize the starch granule hydrolysis,
139 the samples were heated up to 59 °C (PE100, Linkam, UK).
140 However, we choose to focus on 20 °C experiments where the
141 degradation occurred at lower speed and allowed a better
142 amylose 3D tracking. To avoid evaporation of the water from
143 the solution during hydrolysis, the samples were sealed between
144 two quartz coverslips.

145 **Enzymatic Assay.** As described previously,²⁰ 3 mg of maize
146 starch (Roquette Freres, Lestrem, France) was mixed with 10
147 μL of acetate buffer pH 4.5 on a glass plate, and 2 μL of enzyme
148 solution was then added. Purified preparations of RA and AFA
149 were provided as respectively 3 and 4 mg mL⁻¹ solutions in
150 sodium acetate buffer from Novozymes A/S, Denmark. The
151 changes in the granule morphology (visible light) and in the
152 location of amylose (tryptophan fluorescence) were observed at
153 different time scales. In total, six hydrolysis kinetics were
154 imaged with RA and ten with AFA. For each hydrolysis time
155 both visible and fluorescence images were recorded in the full
156 field mode, with at least 20 starch granules per field. The
157 degradation mode was identical for a given amylose but the
158 kinetics were not synchronous for all single granules.

159 **Deconvolution and 3D Representation.** A full-field
160 microscope was chosen for its high detection sensitivity and fast
161 images recording (in comparison to a confocal type micro-
162 scope). In a full-field microscope, the images recorded are
163 contaminated by out-of-focus contributions. However, this can
164 be reduced by deconvolution techniques. The image generated
165 by a microscope is a convolution of the sample with the
166 microscope's point-spread-function (PSF). The PSF describes
167 how a point in the sample is imaged by microscope optics. The
168 brightness of every point in the image is linearly related through
169 convolution to the fluorescence of each point in the object.
170 Consequently, the influence of all optics and filters in the light
171 path can be suppressed by computational optical sectioning
172 microscopy, and a deconvolution algorithm can efficiently
173 reverse the loss of contrast, thus compensating for the blurring
174 effect of defocus. To properly calculate the deconvolution, PSF
175 of the whole system was recorded with calibrated fluorescent
176 beads (TetraSpeck 0.17 μm, Life Technologies, Molecular
177 Probes). This experimental PSF was then applied to the stack
178 of hydrolysis images of starch granule using a deconvolution
179 classical maximum likelihood estimation (Huygens software,
180 SVI, NL) as shown in Figure 1. The step was 500 nm and the
181 acquisition time 10 s.

182 ■ RESULTS AND DISCUSSION

183 Figures 2 and 3 of transmission images show degradation of
184 single maize starch granules during hydrolysis by AFA (from 5
185 to 360 min) and RA (from 10 to 610 min) respectively. As in
186 previous experiments,²⁰ enzymatic breakdown of single starch
187 granules has been monitored but in the present work a larger
188 series of starch granules have been studied (about 20 granules)
189 and during much longer hydrolysis time (up to 20 h in some
190 cases). As far as we know, in the literature, studies of starch
191 granules were conducted only on large populations of granules
192 linking the different degradation stages of hydrolysis^{21–25} with
193 extraction of the most critical changes. Here hydrolysis is
194 directly observed on a series of single starch granules, showing
195 that the process is not synchronous and that at a same
196 hydrolysis time some granules can be greatly degraded while
197 others seem to be intact. RA and AFA differ greatly in the way
198 they degrade the starch granule. In case of AFA, hydrolysis
199 starts from the edges of the granule and the average granule size

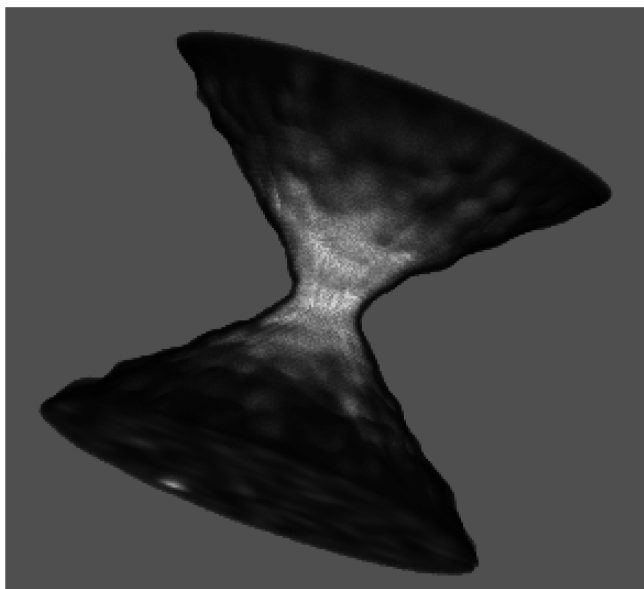


Figure 1. 3D Volume representation of the experimental PSF, using 170 nm fluorescent beads 360/420 (TetraSpeck, Molecular Probes) and distilled by Huygens software (SVI, NL).

200 decreases progressively with increasing hydrolysis time (Figure 201 2). RA hydrolysis starts by the center of the granule, possibly at 202 the hilum, which is poorly structured, rapidly creating some 203 cracks as shown in Figure 3. Hydrolysis then progresses to the 204 edge of the granule leaving a cavity in the center. This different 205 breakdown pathway can probably be linked up to the different 206 biochemical data published on these 2 enzymes.^{17,18} At the end 207 of hydrolysis by RA some smaller thin fragments are observed 208 with a very different texture (Figure 3). The fragments look like 209 a gel or a recrystallized polymer. It could correspond to the B- 210 type structure observed at very high extents of hydrolysis.¹⁷ 211 This structure was shown to originate from recrystallization of 212 linear fragments of macromolecules released by amylase and 213 was present in the end products after hydrolysis.

The location of amylase within the starch granule during 215 hydrolysis by AFA and RA is shown in Figures 4 and 5, 216 respectively, which represent the mapping of tryptophan 217 fluorescence (emission centered around 350 nm) within a 218 starch granule at different optical sections (from -10 to 10 μm 219 using 0.5 μm steps) and at different hydrolysis time (from 5 to 220 360 min). The signal-to-noise ratio is much higher for AFA 221 which contains twice as many tryptophan residues (24 out of 222 584 amino acids) than for RA (11 out of 583 amino acids). 223 Nevertheless the difference in action mode of the two enzymes 224 is clearly evidenced. In case of AFA, the major adsorption of 225 enzyme is on the side of the granule and mostly at the level of 226 the largest diameter where it can be helped by the high specific 227 area induced by the polyhedral shape of the maize starch 228 granule in that region. This specific adsorption is clearly

visualized when looking at the median slices and enzyme seems 229 to be more present in this median section (labeled $z = 0$) than 230 in lower and higher ones. Moreover very little fluorescence is 231 detected on the top and bottom of the granule. This is an 232 artifact of deconvolution that underestimates the quantity of 233 fluorescence from the axial extremities. The quality of images 234 recorded with RA (Figure 5) is lower but it allows a clear 235 evidence of rapid diffusion of enzyme in the central part of the 236 granule toward the inner center. Then, once the center is 237 degraded, RA diffuses toward the more external domains. At 10 238 min hydrolysis, a very strong fluorescence is already observed in 239 the center of granule ($z = 0$) and no clear fluorescence is 240 further observed in the center of the granule after 3 h reaction, 241 fluorescence being shifted toward more external part. At 610 242 min (h), fluorescence is only detected in residual surrounding 243 domains in agreement with the residual morphology shown in 244 Figure 3. A very low fluorescence is last recorded at the end of 245 hydrolysis where only a ghost of the starch granule is 246 remaining. This experiment shows that even with a low 247 signal-to-noise ratio, it is possible to image the location of an 248 enzyme in 3D without any staining or sectioning and for rather 249 low content of tryptophan.

To ensure that the observed fluorescence does not originate 251 from a starch component, fluorescence of a suspension of maize 252 starch granules was studied without amylase. No fluorescence 253 was observed at recording times used for enzyme location (10 254 s) that validates the experiments. At longer recording times 255 (>30 s), a uniform fluorescence background was observed on 256 all granules. This fluorescence was not observed on waxy maize 257 starch, a mutant deficient in GBSS. It shows that observed 258 fluorescence originates from GBSS. It is the first time that 259 GBSS has been imaged in a starch granule, and the results 260 strongly indicate that this biosynthetic enzyme is spread 261 throughout the starch granule. This experiment also shows 262 the sensitivity of the used method to detect a tryptophan- 263 containing component. Seven tryptophans are contained in the 264 whole sequence of GBSS (609 amino acids, $M_w = 66,859$ 265 kDa),¹⁹ that is, tryptophans represent around 2% of the total 266 amount of GBSS. Assuming that the GBSS content is usually 267 less than 0.1% of starch, the sensitivity of the technique is less 268 than 2×10^{-4} .

Figures 6 and 7 show the 3D images of the amylase location 270 and superimposition of their 2D projection with visible images 271 at 3 hydrolysis times, respectively, 5, 135, and 315 min for AFA 272 and 10, 310, and 610 for RA. In that case it is very informative 273 to have the global 3D map of the location of amylase at a given 274 stage of hydrolysis when compared to the 2D images of the 275 granular morphology. Even if the average information is the 276 same (i.e., starting hydrolysis by the periphery for AFA and 277 preliminary degradation of the central core by RA), it yields a 278 very descriptive view of the way amylase progresses within the 279 semicrystalline architecture of the starch granule. The way 280 amylase diffuses in the granule is very homogeneous, 281 evidencing that crystalline domains are not limiting hydrolysis 282

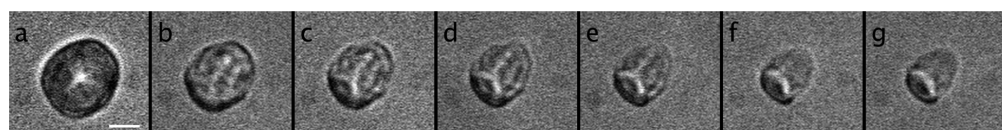


Figure 2. Transmission visible light images of single maize starch granule during hydrolysis by AFA: (a) 5, (b) 45, (c) 90, (d) 135, (e) 180, (f) 315, and (g) 360 min. The scale bar is 5 μm .

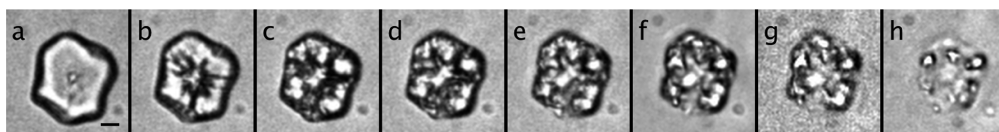


Figure 3. Transmission visible light images of single maize starch granule during hydrolysis by RA: (a) 10, (b) 45, (c) 70, (d) 130, (e) 250, (f) 310, (g) 370, and (h) 610 min. The scale bar is $2\text{ }\mu\text{m}$.

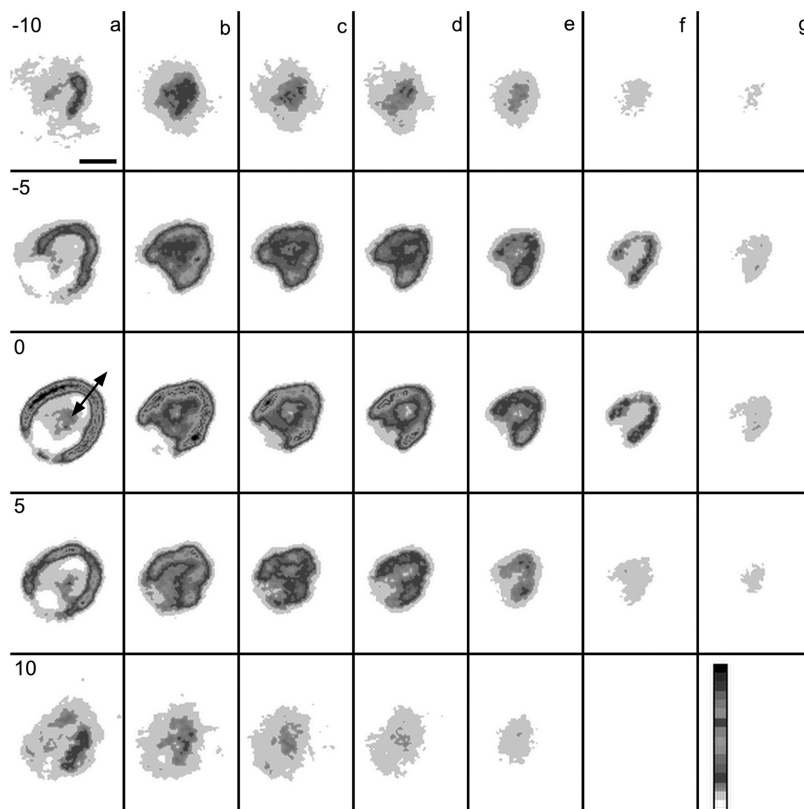


Figure 4. Fluorescence images of amylose on maize starch granule during hydrolysis by AFA (excitation at 280 nm , 10 s acquisition time). The Z vertical axis positions in micrometer are indicated ($-10, -5, 0, +5, +10$): (a) 5, (b) 45, (c) 90, (d) 135, (e) 180, (f) 315, and (g) 360 min. The scale bar is $5\text{ }\mu\text{m}$. The thickness measured of the inner shell (600 nm) is indicated by an arrow.

as already shown from kinetics work.^{17,18} Nevertheless when looking at the surface of 3D images (Video 1), it is not smooth but bumpy that could correspond to local higher resistance to enzyme degradation. Moreover for AFA at 5 min (a) two different layers are clearly evidenced on the bottom right side of image which could correspond to different levels of resistance within the starch granules. This is still more obvious at 135 min (d) where amylose is spread over a much broader distance within the granule. This difference in local susceptibility to amylose attack could be related to the specific architecture of the starch granule which consists of alternating amorphous background and $400\text{--}600\text{ nm}$ semicrystalline growth rings. Finally on the image from 315 min (f) the residual part of the starch granule is still reduced with amylose spread over a much larger thickness in the noncompletely degraded areas. The overall thickness of the starch granule has concomitantly decreased during hydrolysis, which is obvious when looking at both the visible light image and the vertical height of the tryptophan fluorescence 3D map.

As shown in Figure 7 and mentioned above, the action mode of RA is completely different. The 3D mapping of amylose at 10 min (a) illustrates the very rapid diffusion of RA toward the center within the central part of the granule, which is in

accordance with the well-known low level of organization present in that part. Then the diffusion toward the more external areas of the granule seems not to be limited by higher organization and semicrystallinity in more external layers, since the amylose fluorescence is spread over a rather small thickness at 310 and 610 min as well. It would have been impossible to obtain such result from a single 2D mapping as shown in Figure 7 at 310 min (f). This result clearly highlights the real efficiency of the 3D mapping for looking at the amylose diffusion within the granule. Nevertheless it is obvious that on the periphery of the granule some domains are much more resistant to amylose than others since some bumps are interspersed among degraded domains are visible on both light and fluorescence images. The difference in mode of action of RA and AFA is remarkable since on the same substrate AFA starts hydrolysis of the most external domains and degrade them quickly while RA seems to be less efficient in the same part of the granule. It shows that in hydrolysis of solid starch granules, amylose binding is an essential stage since RA and AFA differs primarily by their binding properties. AFA has a natural starch binding domain (SBD belonging to the CBM20 family) attached as an integral part of the catalytic core while RA has a classical SBD (CBM20) linked to the catalytic core by a glycosylated linker.

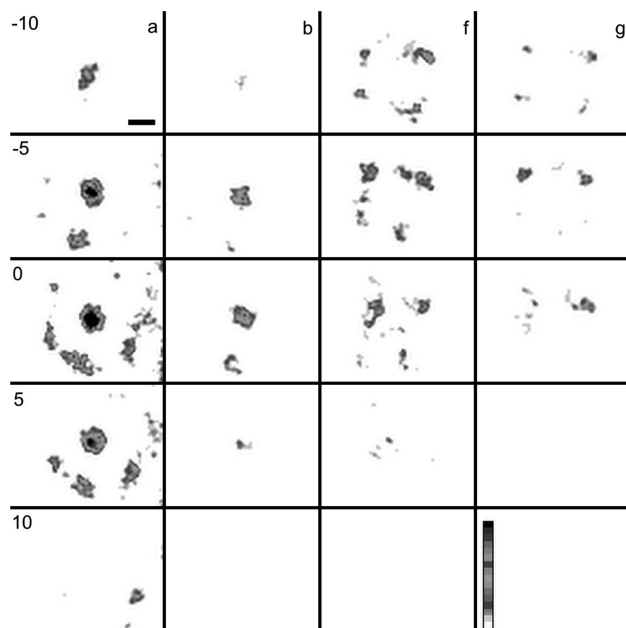


Figure 5. Fluorescence images of amylase on maize starch granule during hydrolysis by RA (excitation at 280 nm, 10 s acquisition time). The Z vertical axis positions in micrometer are indicated ($-10, -5, 0, +5, +10$): (a) 10, (b) 45, (f) 310, and (g) 370 min. The scale bar is 2 μm .

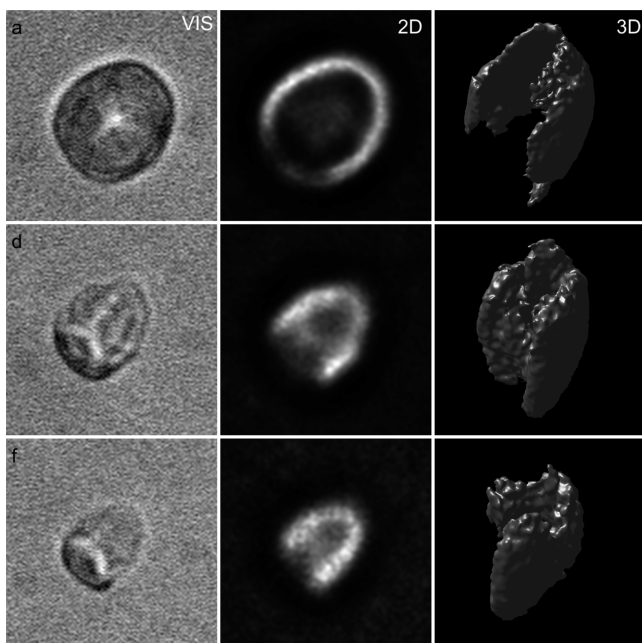


Figure 6. Transmission and corresponding 2D and 3D fluorescence images of the amylose at three different hydrolysis times by AFA ((a) 5, (d) 135, and (f) 315 min).

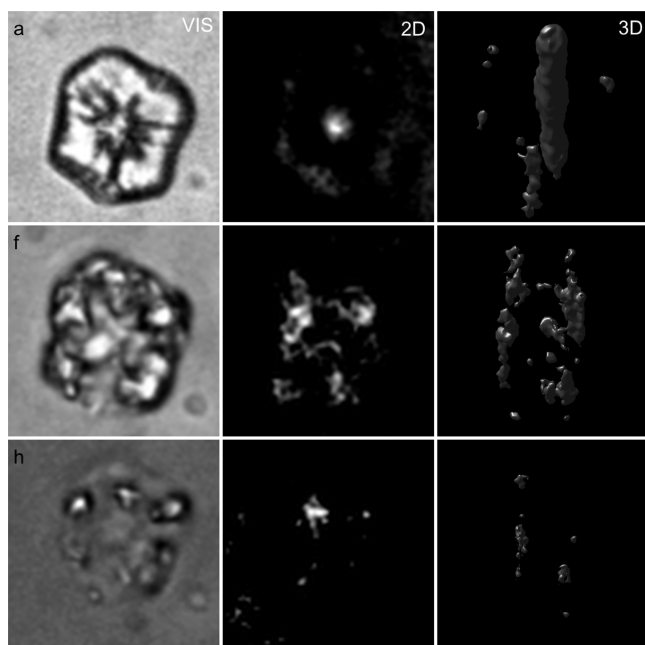


Figure 7. Transmission and corresponding 2D and 3D fluorescence images of the amylase at three different hydrolysis times by RA ((a) 10, (f) 310, and (h) 615 min).

and sectioning. It has been made possible thanks to a unique setup built at synchrotron SOLEIL using fluorescence or luminescence in the VUV wavelength range. Such setup allows following natural fluorescence at much lower wavelength than conventional lasers used for confocal microscopy, as for example that of tryptophan used in this work to map enzymes. The lateral resolution is also increased when looking in the UV range since it depends directly on the excitation wavelength.

It shows that the same type of starch granules can be degraded in a very different pathway by amylases from different sources and that the starch granules are not degraded at the same time. The study of protein dynamics, interactions, and localization at high resolution has always been a major challenge. Enzymology is one of the fields that will benefit greatly when one single protein can be followed when acting on a non-UV-fluorescent substrate. This tool is particularly effective to improve knowledge and understanding of enzymatic hydrolysis of solid substrates including lignocellulosic biomass. It could open the way to new routes in the field of analytical chemistry and sustainable development, as for biotechnology, biorefining, or biofuels.

ASSOCIATED CONTENT

Web-Enhanced Feature

Video representation of AFA at 5, 135, and 315 min and RA at 10, 315, and 615 min is available in the HTML version of this paper.

AUTHOR INFORMATION

Corresponding Author

*E-mail: frederic.jamme@synchrotron-soleil.fr.

Author Contributions

The manuscript was written through contributions of all authors. All authors have given approval to the final version of the manuscript.

This shows that the specificity of these two types of binding domains in combination with the catalytic core are very different with respect to their preferential adsorption sites on the starch granule.

CONCLUSIONS

This work describes the first 3D mapping of amylase within single starch granules, in real time and at different hydrolysis times ranging from few minutes to 10 h, without any staining

370 Notes

371 The authors declare no competing financial interest.

372 ■ ACKNOWLEDGMENTS

373 The SOLEIL synchrotron is acknowledged for beamtime under
374 project # 20110525 and for smooth run of the operations.

375 ■ REFERENCES

- 376 (1) Oates, C. G. *Trends Food Sci. Technol.* **1997**, *8*, 375–382.
377 (2) Gallant, D. J.; Bouchet, B.; Buleon, A.; Perez, S. *Eur. J. Clin. Nutr.*
378 **1992**, *46*, S3–S16.
379 (3) Pohu, A.; Putaux, J. L.; Planchot, V.; Colonna, P.; Buleon, A.
380 *Biomacromolecules* **2004**, *5*, 119–125.
381 (4) Colonna, P.; Leloup, V.; Buleon, A. *Eur. J. Clin. Nutr.* **1992**, *46*,
382 S17–S32.
383 (5) Buleon, A.; Colonna, P.; Planchot, V.; Ball, S. *Int. J. Biol.*
384 *Macromol.* **1998**, *23*, 85–112.
385 (6) Cameron, R. E.; Donald, A. M. *Carbohydr. Res.* **1993**, *244*, 225–
386 236.
387 (7) Banks, W.; Greenwood, C. T. In *Starch and Its Components*, Ed.;
388 Banks, W., Greenwood, C. T., Eds.; Edinburgh University Press:
389 Edinburgh, U.K., 1975; pp 191–241.
390 (8) Yamamoto, T. In *Handbook of Amylases and Related Enzymes*;
391 Amylase Research Society of Japan, Pergamon Press: New York, 1988;
392 pp 18–75.
393 (9) Svensson, B. *Denpun Kagaku* **1991**, *38*, 125–135.
394 (10) Gerard, C.; Colonna, P.; Buleon, A.; Planchot, V. *J. Sci. Food*
395 *Agric.* **2001**, *81*, 1281–1287.
396 (11) Gernat, C.; Radosta, S.; Anger, H.; Damaschun, G. *Starch/*
397 *Staerke* **1993**, *45*, 309–314.
398 (12) Kwasniewska-Karolak, I.; Nebesny, E.; Rosicka-Kaczmarek, J. J.
399 *Food Sci. Technol. Int.* **2008**, *14*, 29–37.
400 (13) Lauro, M.; Forssell, P. M.; Suortti, M. T.; Hulleman, S. H.;
401 Poutanen, K. S. *Cereal Chem.* **1999**, *76*, 925–930.
402 (14) Manelius, R.; Qin, Z.; Avall, A. K.; Andtfolk, H.; Bertoft, E.
403 *Starch/Staerke* **1997**, *49*, 142–147.
404 (15) Planchot, V.; Colonna, P.; Buleon, A. *Carbohydr. Res.* **1997**, *298*,
405 319–326.
406 (16) Viksø-Nielsen, A.; Andersen, C.; Liu, J. Int. Patent
407 WO2007144424-A2, 2009.
408 (17) Tawil, G.; Viksø-Nielsen, A.; Rolland-Sabate, A.; Colonna, P.;
409 Buleon, A. *Biomacromolecules* **2011**, *12*, 34–42.
410 (18) Tawil, G.; Viksø-Nielsen, A.; Rolland-Sabaté, A.; Colonna, P.;
411 Buléon, A. *Carbohydr. Polym.* **2012**, *87*, 46–52.
412 (19) Viksø-Nielsen, A.; Andersen, C.; Hoff, T.; Pedersen, S.
413 *Biocatalysis and Biotransformation* **2006**, *587*, 121–127.
414 (20) Tawil, G.; Jamme, F.; Refregiers, M.; Viksø-Nielsen, A.;
415 Colonna, P.; Buleon, A. *Anal. Chem.* **2011**, *83*, 989–993.
416 (21) Giuliani, A.; Jamme, F.; Rouam, V.; Wien, F.; Giorgetta, J. L.;
417 Lagarde, B.; Chubar, O.; Bac, S.; Yao, I.; Rey, S.; Herbeaux, C.;
418 Marlats, J. L.; Zerbib, D.; Polack, F.; Réfrégiers, M. *J. Synchrotron*
419 *Radiat.* **2009**, *16*, 835–841.
420 (22) Edelstein, A.; Amodaj, H.; Hoover, K.; Vale, R.; Stuurman, N.
421 *Curr. Protoc. Mol. Biol.* **2010**, *14.20.1*–*14.20.17*.
422 (23) Helbert, W.; Schulein, M.; Henrissat, B. *Int. J. Biol. Macromol.*
423 **1996**, *19*, 165–169.
424 (24) Thomson, N. H.; Miles, M. J.; Ring, S. G.; Shewry, P. R.;
425 Tatham, A. S. *J. Vac. Sci. Technol. B* **1994**, *12*, 1565–1568.
426 (25) Apinan, S.; Yuijiro, I.; Hidefumi, F.; Takeshi, F.; Myllarinen, P.;
427 Forsell, P.; Poutanen, K. *Starch/Staerke* **2007**, *59*, 543–548.